scientific reports

Check for updates

OPEN

Observed kinetics for the production of diethyl carbonate from CO_2 and ethanol catalyzed by CuNi nanoparticles supported on activated carbon

Oscar Felipe Arbeláez Perez[1], Felipe Bustamante Londoño[2], Aída Luz Villa Holguin[2], Alba N. Ardila A.[3]✉ & Gustavo A. Fuentes[4]

Monometallic and bimetallic Cu:Ni catalysts with different Cu:Ni molar ratios (3:1, 2:1, 1:1, 1:2, 1:3) were synthesized by wetness impregnation on activated carbon and characterized by TPR (temperature programmed reduction), XRD (X-ray diffraction) and XPS (X-ray photoelectron spectroscopy). The synthesized catalysts were evaluated in the gas phase production of diethyl carbonate from ethanol and carbon dioxide. The largest catalytic activity was obtained over the bimetallic catalyst with a Cu:Ni molar ratio of 3:1. Its improved activity was attributed to the formation of a Cu–Ni alloy on the surface of the catalyst, evidenced by XPS and in agreement with a previous assignment based on Vegard law and TPR analysis. During the reaction rate experiments, it observed the presence of a maximum of the reaction rate as a function of temperature, a tendency also reported for other carbon dioxide–alcohol reactions. It showed that the reaction rate-temperature data can be adjusted with a reversible rate equation. The initial rate as a function of reactant partial pressure data was satisfactorily adjusted using the forward power law rate equation and it was found that the reaction rate is first order in CO_2 and second order in ethanol.

Keywords Carbonate synthesis, Catalytic processes, Ethanol transformation, CO_2 emissions, Value added product

Fast growing population and unrestrained usage of natural resources are the major contributors for carbon dioxide emissions into the atmosphere [1]. There are different methodologies to transform carbon dioxide (a cheap, recyclable and non-toxic carbon source) into useful chemical compounds [2]. These include syngas (from CO_2 and CH_4) [3], methanol (from CO_2 and H_2) [4], urea (from ammonia and CO_2) [5] among others. CO_2 can also form linear carbonates, such as dimethyl (DMC) and diethyl carbonate (DEC), by its reaction with methanol [6] or ethanol, respectively [7]. DEC is becoming increasingly important in the chemical industry; it is mainly used as an electrolyte in lithium-ion batteries [8] and as a fuel additive [9]. In organic synthesis, DEC is used as a solvent, and as a carbonylation and alkylating agent due to the presence of CH_3CH_2O– and –CO– groups [10]. The synthetic route from CO_2 and ethanol to produce diethyl carbonate and water, avoids the problems caused by the use of toxic, corrosive and flammable gases in the standard synthesis routes, i.e., phosgene and hydrogen chloride (ethanolysis of phosgene [11], carbon monoxide (oxidative carbonylation of ethanol [12]), or ethyl nitrite (carbonylation of ethyl nitrite [13]), diethyl oxalate (decarbonylation of diethyl oxalate [14]) and propylene carbonate [15]. There is low DEC selectivity in some of these routes, e.g., propylene oxide, ethanol and carbon dioxide transesterification [16], ethanolysis of urea [17–19], and ethanol and dimethyl carbonate transesterification [20].

[1]Grupo de investigación Termomec, Facultad de Ingeniería, Universidad Cooperativa de Colombia, Calle 50 No. 40-74 - Bloque A - Piso 4, Medellín, Colombia. [2]Environmental Catalysis Research Group, Chemical Engineering Department, School of Engineering, Universidad de Antioquia, Calle 70 No. 52-21, Medellín, Colombia. [3]Research Group in Environmental Catalysis and Renewable Energies, Facultad de Ciencias y Educación, Politécnico Colombiano Jaime Isaza Cadavid, Apartado Aéreo 49-32, Medellín, Colombia. [4]Department of Process Engineering, Universidad Autónoma Metropolitana-Iztapalapa, San Rafael Atlixco 186, 09310 Mexico, DF, Mexico. ✉email: anardila@elpoli.edu.co

Several catalysts have been reported for the production of DEC starting from ethanol and CO_2 (Table 1). The most common catalyst evaluated for DEC synthesis in the liquid phase are CH_3CH_2I–K_2CO_3 [21], K_2CO_3 [22], CeO_2 [23], $Ce_xZr_{1-x}O_2$ [24], CeO_2-SiO_2 [25] and ZrO_2 [26].

The catalytic activity for DEC formation is generally very low, because of the high thermodynamic stability and inert nature of carbon dioxide. Reports in the literature about DEC production in the liquid phase have focused on the effect of catalysts on activity and product distribution as a function of reaction pressure and temperature. An increase of catalytic activity (DEC yield) with reaction temperature was reported by Yoshida et al. [23] and Wang et al. [27] over CeO_2 and $CeZrO_2$ catalysts, respectively. Additionally, Prymak et al. [24] reported that the liquid phase reaction was favored at low temperature and high pressure. Those conditions caused rapid catalyst deactivation [28].

We previously reported the successful use of Cu, Ni and Cu–Ni supported on activated carbon [29] and ZrO_2 [30] as catalysts for the gas phase synthesis of DEC starting from ethanol and CO_2 at moderate pressure (13 bar) and temperature (363 K). The Cu monometallic catalyst was three times more active (turnover frequency (TOF) = 5.1 h^{-1}) than the monometallic Ni catalyst (TOF = 1.6 h^{-1}). The catalytic activity increased further when both Cu and Ni were present in the catalyst, and the DEC rate increased with the Cu:Ni ratio. The TOF increased nearly 12 and 25 times for Cu:Ni molar ratios of 2:1 (53 h^{-1}) and 3:1 (126 h^{-1}), respectively. The enhanced catalytic activity over bimetallic catalysts was ascribed to the presence of Cu–Ni alloys on the surface of AC, which assignment was based on X-ray diffraction and TPR analysis.

As far as the authors know, there is no information about the effect of reaction parameters (temperature and pressure) on the gas-phase production of DEC. We report here the effect of temperature and pressure on the activity of Cu–Ni/AC catalyst. XPS analysis of Cu–Ni/AC evidence the presence of surface Cu–Ni alloys, presumably responsible for the increased activity of those catalysts. Additionally, a kinetic equation for the direct synthesis of DEC from ethanol and carbon dioxide is proposed.

Materials and methods

Catalyst preparation

Activated carbon AC supplied by Merck (90%, particle size < 100 μm) was used as support and the catalysts were synthesized by wetness impregnation. The metal precursors used were Cu(NO3)2·3H_2O (supplied by Carlo Erba 99.5%) and Ni(NO3)2·6H_2O (supplied by Merck 99%). A nominal 20% wt. loading of metal oxide (CuO + NiO) was used. Samples with different Cu:Ni molar ratios: 3:1, 2:1, 1:1, 1:2, and 1:3 were prepared. The metal precursors were dissolved in distilled water and mixed with the support for 24 h. The materials were then roto-evaporated for 3 h. The resulting samples were dried at 363 K for 12 h and calcined under a flow of 25 mL min^{-1} of N_2 at 773 K for 3 h using a heating rate of 0.5 K min^{-1}. The catalysts were finally reduced in a 5% H_2/Ar mixture at 873 K.

Catalytic activity

Catalytic activity was evaluated using 1.0 g of catalyst in a cylindrical stainless steel fixed-bed reactor (internal diameter 0.7 cm). Ethanol was injected into the reactor by flowing a stream of He/CO_2 at the appropriate flow rate through a stainless-steel bubbler containing liquid ethanol supplied by Merck (96%). The CH_3CH_2OH:CO_2 molar ratio and partial pressures were regulated by saturating the stream with ethanol at different temperatures and by changing the He/CO_2 ratio. A hot box system equipped with a K-type thermocouple was used to control the reaction temperature; additionally, a heating system was used to keep constant the outlet temperature at 420 K, avoiding possible condensation. After each catalytic test, argon gas was flowed (50 mL min^{-1}) through the reactor for 24 h to clean the reaction system. Ethanol (m/z = 30), carbon dioxide (m/z = 22), DEC (m/z = 91) and diethyl ether (m/z = 74) were monitored online with a mass spectrometer (QMS Thermostar 200, Pfeiffer).

Kinetic tests were performed with different catalyst particle sizes and feed space times W/F_{ETOH} (50–130 g h mol^{-1}) using 1.0 g of the best catalyst, a 2:1 molar ratio ethanol: carbon dioxide as a reactant mixture, and 13 bar total pressure. Temperature ($383 \le T \le 463$ K) and partial pressure of reactants ($0.2 \le P_{ETOH} \le 0.34$ bar, $0.32 \le P_{CO2} \le 1.31$ bar) were varied in the catalytic tests. The temperature and pressure range were selected in accordance previous studies [31].

As the ethanol conversion was low throughout our study, we could assume differential operation for the experimental reactor, which allowed us to estimate the catalytic activity using Eqs. 1 and 2.

Catalyst	Temperature (K)	Pressure (bar)	Y_{DEC} (%)	S_{DEC} (%)	Reference
CH_3CH_2I–K_2CO_3	343	80	0.15	n.r	[21]
K_2CO_3	383	20	5.00	67	[22]
CeO_2	383	50	0.19	n.r	[23]
$Ce_xZr_{1-x}O_2$*	413	80	0.10	94	[27]
$Ce_xZr_{1-x}O_2$†	413	140	0.7	n.r	[24]
CeO_2–SiO_2	453	45	0.08	n.r	[25]
ZrO_2	423	8.3	0.53‡	39	[26]

Table 1. Heterogeneous catalysts reported for DEC synthesis in the liquid phase. n.r. not reported. Ce content, *x = 0.07, †x = 0.8. Y_{DEC}: DEC yield, S_{DEC}: DEC selectivity. ‡mmol de DEC.

$$r_{DEC} = \frac{F_{DEC}}{W} \tag{1}$$

$$S_{DEC} = \frac{F_{DEC}}{F_{DEC} + F_{DEE}} \times 100 \tag{2}$$

where W = the catalyst weight (g), r_{DEC} = rate of reaction (mol g^{-1}_{cat} min^{-1}) of DEC, S_{DEC} = DEC selectivity, F_{DEC} = molar flow of DEC, F_{DEE} = molar flow of diethyl ether.

Catalyst characterization

Chemical composition

Chemical composition of the catalysts was determined by atomic absorption spectroscopy in a Philips PU9200 spectrometer with a rhodium radiation source operating at 40 kV; 0.5 g of the catalyst were digested in $HCl–HNO_3$ solution for the analysis.

X-ray diffraction (XRD)

X-ray diffraction (XRD) analysis was performed on a Phillips PW 1740 diffractometer. Diffraction patterns were recorded with Cu Kα radiation (20 mA, 40 kV) over a 5°–70° 2θ-range. The XRD patterns were compared with JCPDS files. The Scherrer Eq. (3), was used to calculate the crystallite size.

$$D = \frac{K\lambda}{(\beta_m - \beta_i)\mathrm{Cos}(\theta)} \tag{3}$$

Here, D: size of the crystallite (nm), K: Scherrer constant, which is equal to 0.94 for spherical crystals, λ: radiation wavelength (0.154 nm), $(\beta_m - \beta_i)$ is the broadening of the full width at half maximum of the main peak, β_m: sample; β_i: reference = 0.11, θ is the Bragg angle (degrees).

Temperature programmed reduction (TPR)

Temperature programmed reduction analysis of the samples was measured in a Micromeritics AutoChem II 2920. 50 mg of the sample were first heated from 278 to 523 K and kept at that temperature for 1 h in 70 mL min^{-1} He flow before cooling down to 313 K. The samples were then heated from 281 to 1073 K in 70 mL min^{-1} 5% H_2/Ar mixture flow.

Transmission electron microscopy (TEM)

A transmission electron microscope (JEOL 2010) operating at 200 kV and 124 μA was used to determine the morphology, size, and size distribution of metallic particles as it was reported by Tayyab et al. [32].

X-ray photoelectron spectroscopy XPS

The XPS measurements were collected with a spectrometer (Thermo VG Scientific Escalab 250) operated at 20 kV and 30 mA. All catalysts were reduced in flowing H_2 at 593 K for 30 min before the XPS measurements. The binding energy (BE) of the C 1s peak was used as an internal standard. Relative concentrations of metals were estimated by calculating the integral of each XPS peaks using the cross sections [33].

Results and discussions

Catalytic activity

Figure 1 shows the catalytic activity (expressed as DEC reaction rate) during DEC synthesis at 383 K. The total Cu content varied from 0 to 100% and Cu:Ni molar ratio ranged from 1:1 to 3:1. The catalytic activity of monometallic samples was also evaluated.

There was no CO_2 conversion when no catalyst was loaded neither when tests were carried out with activated carbon. The monometallic Cu catalyst exhibited higher catalytic activity (1.6×10^{-5} mol g^{-1}_{cat} min^{-1}) than the Ni monometallic catalyst (0.7×10^{-5} mol g^{-1}_{cat} min^{-1}). This result is according with reports by Bian et al. [34], for the formation of dimethyl carbonate. Deng et al. [35] used surface enhanced Raman spectroscopy and suggested that Cu can activate CO_2 by forming negatively charged $CO_2^{\delta-}$ species, which can further convert to carbonate. The corresponding Raman bands were reported at 767 cm^{-1} (bending mode δ(OCO)) and at 1182 cm^{-1} (symmetric stretch mode). Figure 1 shows the DEC reaction rate as function of Cu:Ni molar ratio of our bimetallic catalysts. As a result of the Cu–Ni interaction the reaction rate for the bimetallic catalysts increased significantly when compared with the monometallic. The increase in the catalytic activity as a function of the Cu molar ratio agrees with data reported by Bian et al. [34] during linear carbonate synthesis in this composition range. In our case, the reaction rate increased about 2 and 2.5 times for Cu:Ni molar ratios of 2:1 and 3:1, respectively, when compared with the activity of the Cu/AC catalyst. The interaction between Cu and Ni also decreased the production of CO and improved the catalyst resistance to coke formation [36].

The selectivity to diethyl carbonate ranged between 82 and 88%, and it is similar to the values reported by Bian et al. [34] for the formation of dimethyl carbonate from methanol and carbon dioxide. The main side product was diethyl ether, that probably is produced by decomposition of DEC, rather than by dehydration of ethanol. This was verified by feeding either ethanol or diethyl ether to the reactor packed with 1.0 g of Cu:Ni/AC catalyst with a Cu:Ni molar ratio of 3:1, and operating at 13 bar and 383 K. The dehydration of ethanol has been reported to occur at 423 K, but in the presence of basic catalysts [17].

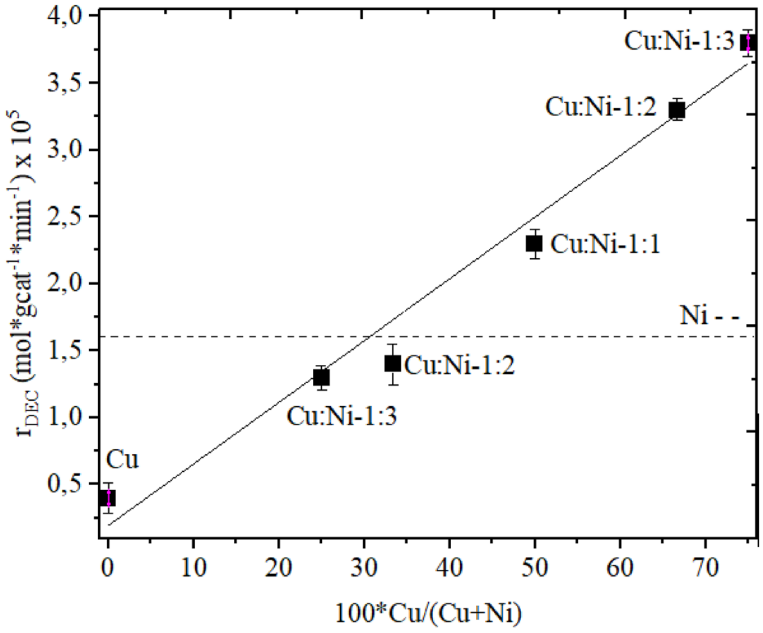

Figure 1. Catalytic activity of tested catalysts. Reaction conditions: 383 K, 13 bar, ethanol: CO_2 feed molar ratio of 2:1, gas hourly space velocity of 988 h^{-1}.

Effect of catalytic reaction conditions on DEC reaction rate

Effect of mass transfer limitations

The conditions in which there were no external or internal mass transfer resistances were identified. Figure 2 shows that DEC reaction rate remained constant when the flowrate was higher than 75 mL min^{-1}, indicating the absence of external gas phase mass transfer resistance. Experiments with different catalyst particle sizes were performed to verify the absence of intraparticle mass transfer resistance. Figure 3 shows that the reaction is free of intraparticle mass transfer limitations for particle sizes below about 300 μm.

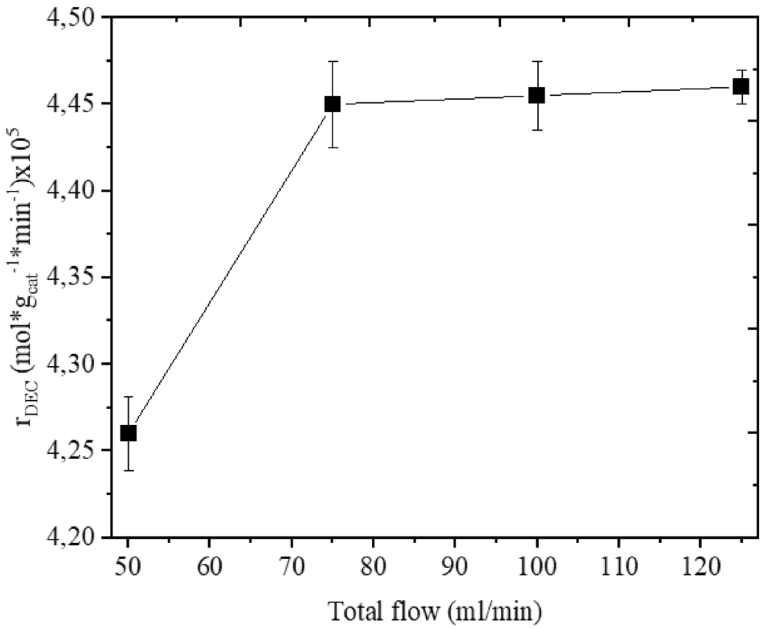

Figure 2. Analysis of external mass transfer limitations. Reaction conditions: 383 K, total pressure: 13 bar, catalyst weight: 1.0 g, ethanol:CO_2 feed molar ratio of 2:1.

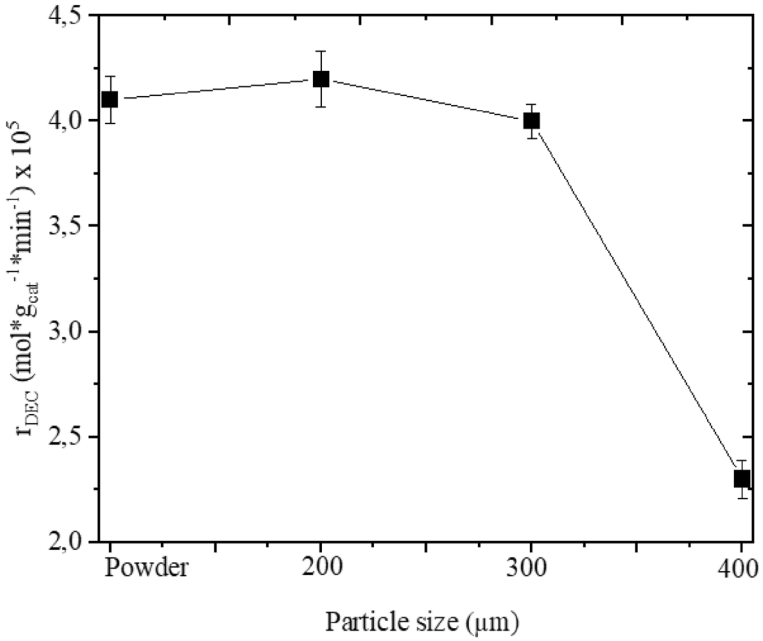

Figure 3. Analysis of internal mass transfer limitations. Reaction conditions: 383 K, total pressure: 13 bar, catalyst weight: 1.0 g, ethanol: CO_2 feed molar ratio of 2:1.

Effect of reaction temperature

When the effect of temperature was tested, it was found that the DEC reaction rate increased with temperature from 343 K until it reached a maximum value at 383 K, decreasing continuously afterwards (Fig. 4). This effect suggests that an equilibrium restriction is involved, given the exothermic nature of the reaction [31]. The presence of a maximum in rate in the 363–393 K range was reported by Orrego et al. [37], Chen et al. [38], and Bian et al. [34,39,40] for different alcohol–CO_2 reactions.

The decrease of reaction rate at high temperature has been associated to blockage by CO_2 adsorption [40], but that is not likely to be the case, as adsorption normally decreases when temperature increases. Furthermore,

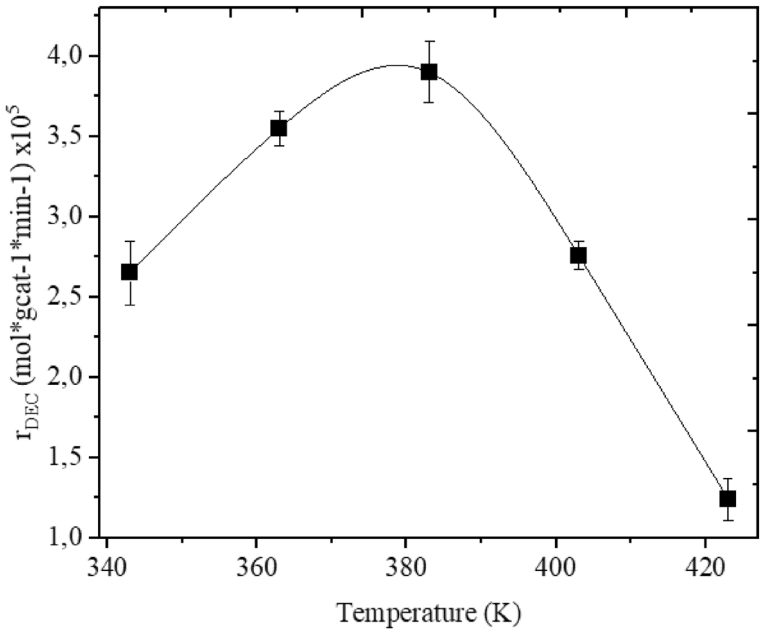

Figure 4. Reaction temperature effect. Reaction conditions: Total pressure: 13 bar, 1.0 g Cu:Ni-3:1, total flow: 75 mL min^{-1}, ethanol: CO_2 feed molar ratio of 2:1.

the decrease in DEC yield as a function of temperature was associated to a probable enhancement of catalyst deactivation at high temperatures and to an increased reactant mass throughput [41].

Pressure dependence of the reaction rate

The proposed kinetic equation and the estimated fitting parameters, as well as the corresponding standard errors are given in Table 2.

The power law equation provides a good fit ($r^2 = 0.954$) of the experimental results and appears to be an adequate alternative to represent pressure and temperature dependence of the rate (supplementary information). The proposed rate equation presented in this study is the first one proposed for this class of reactions, i.e., reaction in gas phase between CO_2 and an aliphatic alcohol. The kinetic equations reported by other authors for DEC synthesis are reported in Table 3.

Kinetics studies for DEC synthesis from ethanol and carbon dioxide are scarce. Table 3 shows kinetic equations reported in open literature for DEC synthesis from ethanol and carbon dioxide. Décultot et al. [42] reported a kinetic equation for the reversible reaction using a model based on Langmuir–Hinshelwood mechanism for the reaction in liquid phase. Power law model was used for describing the kinetic of the reverse and forward reactions under multiphase conditions and used for the plant-wide process to produce diethyl carbonate from the direct reaction of CO_2 with ethanol, using 2-cyanopyridine as an in situ dehydrating agent [42], and also reported by Giram et al. using CeO_2 as catalyst [43]. As the phases of the reaction influence the final kinetic equation, the reported rate equations cannot be compared.

Catalysts characterization

XRD results

Figure 5 presents the diffractograms of Cu/AC and Ni/AC with reflections at $2\theta = 43.3°$ and 50.4° that correspond to the (111) and (200) planes of Cu^0 face cubic centered cell (JCPDS 4-0836) and reflections at $2\theta = 44.5°$ and 51.8° that correspond to 111 and 200 planes of Ni^0 face cubic centered cell (JCPDS 4-0850). In Cu–Ni bimetallic samples an increase in Cu loading caused a linear shift of the (111) and (200) diffraction lines. A linear relationship between the lattice parameter and the Cu concentration agrees with Vegard law [44], and is a strong evidence of the formation of a Cu–Ni solid solution [45]. The improved catalytic activity for DEC formation observed with the 3:1 and 2:1 catalyst appears to be related to the presence of such Cu–Ni alloy. Cu, Ni and Cu:Ni-3:1 mean particle size was estimated using Scherrer equation (Eq. 3). The particle size of the bimetallic Cu:Ni-3:1 sample was 22.2 nm, a value between those calculated for Cu (23.5 nm) and nickel (17.3 nm) monometallic samples.

Temperature programmed reduction

TPR profiles of the catalysts are presented in Fig. 6. Activated carbon has a single broad reduction signal above 873 K. The reduction patterns of the metal-containing samples have significant differences in the low to medium temperature range (473–673 K). The monometallic Cu catalyst exhibits one reduction peak centered at 524 K assigned to the reduction of bulk CuO [34]. The monometallic Ni supported catalyst has two reduction signals; the low temperature signal has a maximum at 554 K with a shoulder at 515 K, and is assigned to the reduction of NiO species with different degrees of dispersion [46]. The high temperature reduction peak has a maximum at 653 K and is attributed to the reduction of "free" NiO with activated carbon during the thermal treatment [47].

Kinetic equation	Estimated value	Standard error
$r_{DEC} = kP_{ETOH}^2 P_{CO_2}$	$k = 3.503 \times 10^{-7}$	2.71574×10^{-8}

Table 2. Power law model and kinetic parameters for DEC formation at 13 bar total pressure and 383 K. k [mol g_{cat}^{-1} min^{-1} bar^{-3}].

Kinetic equations	k, Ea	Other constants	References
$r_A = k_A \frac{\left(\frac{[EtOH]^2 P_{CO_2}}{C_0^2 P_0} - \frac{[DEC][H_2O]}{K_{eq} C_0^2}\right)}{\left(1 + K_{A1}\frac{P_{CO_2}}{P_0} + K_{A2}\frac{[EtOH]}{C_0} + \frac{[DEC]}{C_0 K_{A4}} + \frac{[H_2O]}{C_0 K_{A5}}\right)^3}$ $CO_2 + 2(EtOH) \leftrightarrow DEC + H_2O$ Liquid phase	$k_{0A} = 3.61 \times 10^{10}$ mol/L/h Ea = 101 kJ/mol	$K_{A1} = 0.096$, $K_{A2} = 0.051$, $K_{A4} = 0.028$, $K_{A5} = 0.014$	15
$r_1 = k_1 \exp(-Ea_1/RT)$ $CO_2 + 2(EtOH) \rightarrow DEC + H_2O$ Multiphase	$k_1 = 4.608 \times 10^{14}$ kmol/kgcat.s Ea = 150,163 kJ/mol		42,43
$r_2 = k_2 \exp(-Ea_2/RT) X_{DEC} X_{H2O} / X_{CO2} X_{EtOH}^2$ $DEC + H_2O \rightarrow CO_2 + 2(EtOH)$ Multiphase	$k_2 = 5.550 \times 10^{17}$ kmol/kgcat.s Ea = 125,359 kJ/mol		42,43

Table 3. Kinetic equations reported in literature for DEC synthesis. P^0 and C^0 represent the standard pressure and concentration equal to 1 bar and 1 mol/L, respectively. Xi: mole fraction of components. Ea: apparent activation energy.

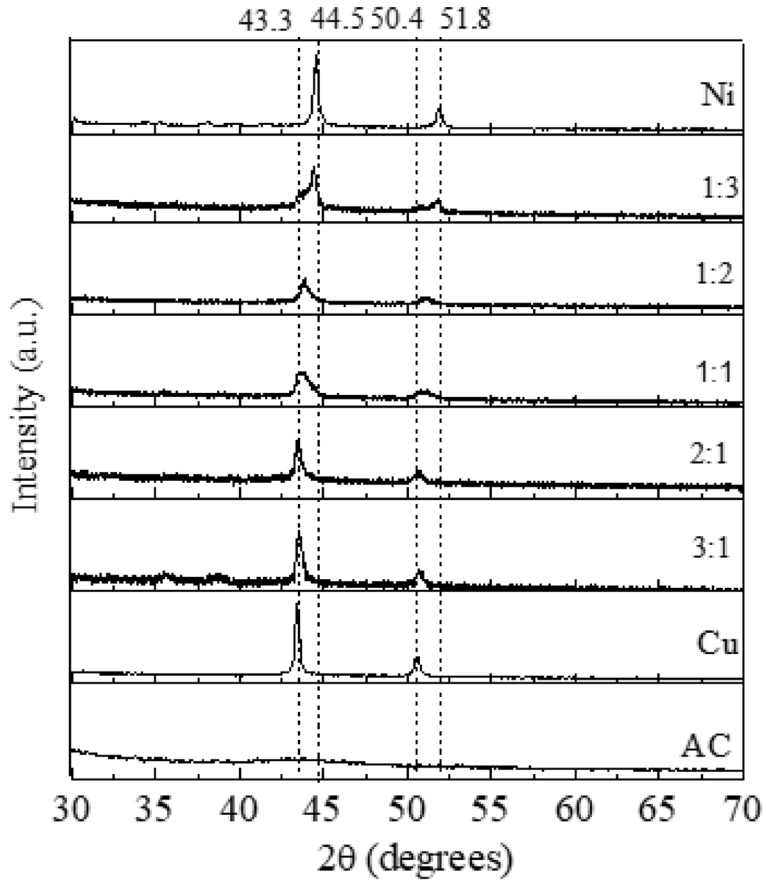

Figure 5. XRD of tested catalysts.

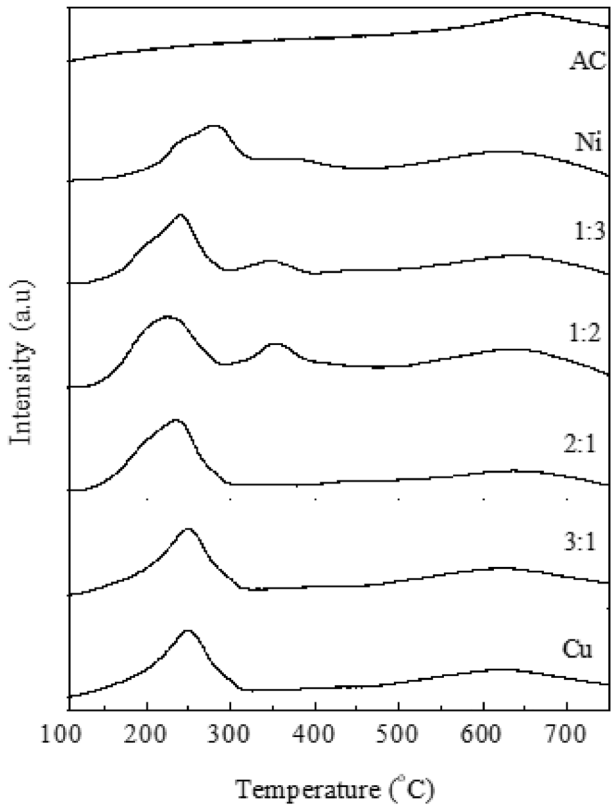

Figure 6. TPR of support, Cu, Ni and bimetallic Cu:Ni at different molar ratios.

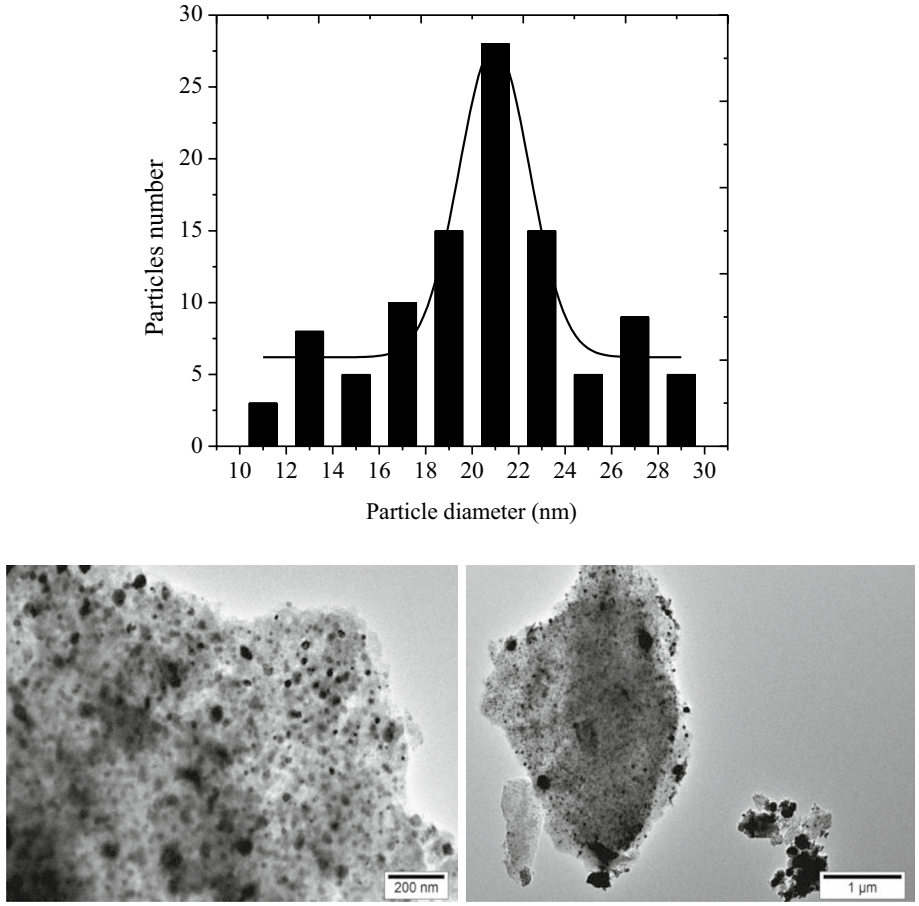

Figure 7. TEM particle distribution of Cu:Ni-3:1. Light zones (support) and dark zones (metal particles).

In addition, the reduction temperatures of monometallic catalysts were higher than those for the unsupported monometallic CuO (486 K) and lower than those for NiO (631 K). The supported bimetallic catalysts with low Cu content had reduction patterns that combined those of the monometallic samples; however, the catalysts with the higher Cu content (Cu: Ni-2:1 and Cu:Ni-3:1) had a single reduction peak similar to the Cu sample. This clearly indicates that Ni reduction is strongly promoted by the interaction with Cu, and is another evidence of the formation of new phases between Cu and Ni, which was also confirmed by XRD. Our results agree with the report of Khromova et al. [45], who attributed the more facile reduction of CuO in the bimetallic Cu–Ni samples to the lower free energy of reduction for CuO (− 100.65 kJ mol^{-1} at 293 K) compared with NiO (− 12.31 kJ mol^{-1} at 293 K). The TPR profiles evidence a high synergy between Cu and Ni that may have an impact on DEC formation. All the samples show also a broad H_2 consumption band at temperature higher than 773 K caused by the C–H_2 reaction to form CH_4 (observed also with pure activated carbon); however, the hydrogen activation does not affect the activity for DEC production, as the latter reaction occurs at much lower temperatures.

TEM analysis

Figure 7 shows the TEM images and particle-size of Cu:Ni-3:1 sample.

The TEM images show the morphological characteristics of the Cu:Ni-3:1 catalyst. In bimetallic samples, particles (dark zones) adopt spherical, rectangular, elliptical and irregular shapes as is reported by activated carbons [34], carbon nanotubes [40], nanowires [46], graphitic carbon [48] and ZnO–ZnS [49]. Figure 7 shows a homogeneous distribution of metal particles over the carbon support, with some agglomerates observed in Cu–Ni sample. The particle size of the small nanocrystals of Cu–Ni alloy was 21 nm, in good agreement with XRD results. The diameter of Cu–Ni alloy is close to a simple addition of the diameters of Cu and Ni which suggests a possible insertion of Ni into Cu structure.

XPS analysis

The XPS spectra for Cu and Ni monometallic catalysts are presented in Figs. 8 and 9, respectively; results are compared with Cu:Ni-3:1 catalyst in both cases.

Figure 8a depicts the XPS spectra in the Cu 2p region for Cu and Fig. 8b Cu:Ni-3:1 bimetallic catalyst. Monometallic sample, Fig. 8a, shows two peaks at approximately 932.8 eV and 952.8 eV assigned to Cu2p3/2 and Cu2p1/2, respectively, indicating the zero-oxidation state of Cu after the reduction process, and a spin–orbit

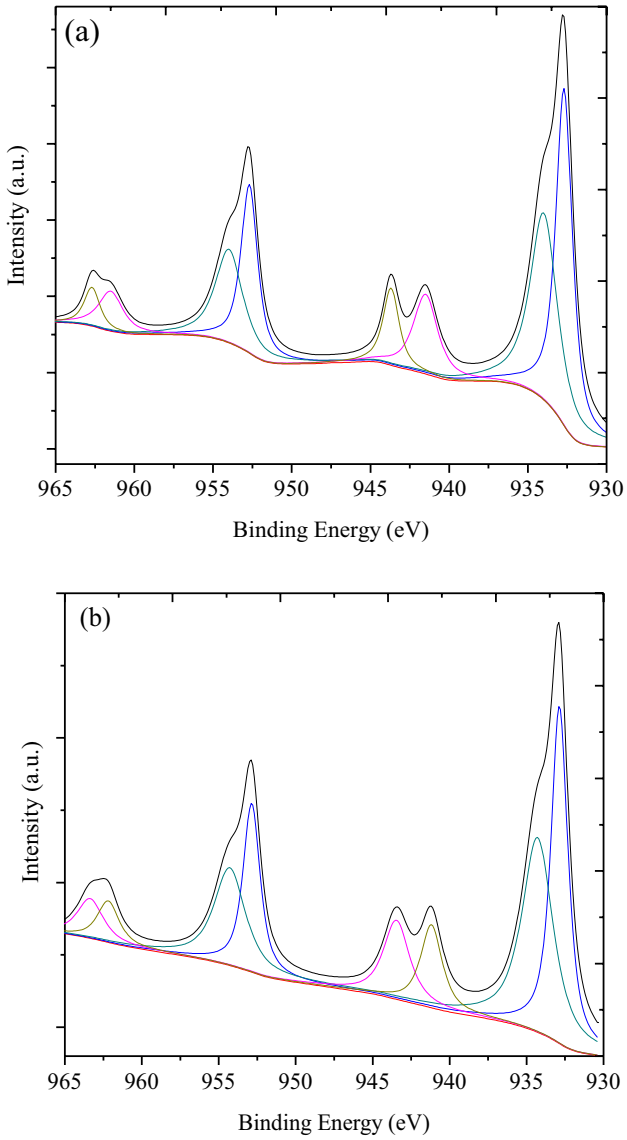

Figure 8. Cu2p core-level spectra: (**a**) Cu catalyst and (**b**) Cu:Ni-3:1 catalyst.

coupling energy of 20 eV and two strong satellite peaks at 944.2 eV and 962.6 eV. Experimental results indicate that copper is in the Cu^0 or Cu^{1+} and Cu^{2+} states. The presence of Cu^0 and Cu^{1+} was confirmed by a main peak in the 932.4–932.8 eV range associated with Cu2p3/2, while the presence of CuO was confirmed by high-intensity shake-up satellites at approximately 9–12 eV higher binding energy than the main Cu2p3/2 and Cu2p1/2 peaks. In bimetallic sample, Fig. 8b, binding energy shift was observed from 932.8 to 933.2 eV. The experimental results indicate that when Cu^{2+} is mixed with Ni, the monometallic catalyst becomes partially reduced, in agreement with TPR results.

The Ni monometallic catalyst (Fig. 9a) exhibits peaks at 854.1 eV (Ni 2 p3/2) and 872.6 eV (Ni 2 p1/2) which confirmed the presence of Ni metal and NiO, respectively. In Cu:Ni-3:1 sample (Fig. 9b) binding energy presents a shifting for Ni 2p3/2 from 854.1 to 856.2 eV, and from 932.8 to 933.2 eV for Cu 2p3/2. According to our experimental results, in the bimetallic sample part of Cu and Ni were in zero oxidation state. Additionally, a slight shifting in the binding energy of Cu and Ni indicated a change in the chemical environment of species related with formation of Cu–Ni alloy [50].

Conclusions

In this work, activated carbon supported Cu, Ni and Cu:Ni catalysts were prepared and tested for the gas phase formation of diethyl carbonate from ethanol and carbon dioxide. Based on the experimental results, it can be concluded that reaction rate of the bimetallic samples increases with the Cu content; Cu:Ni-3:1 molar ratio sample was the most active catalyst. The presence of Cu–Ni alloy was evidenced by XRD, TPR, and XPS analysis. The improved catalytic activity for the production of DEC over Cu:Ni bimetallic materials appears to be caused by the formation of Cu–Ni alloy nanoparticles with electronic and reducibility properties different to those of the

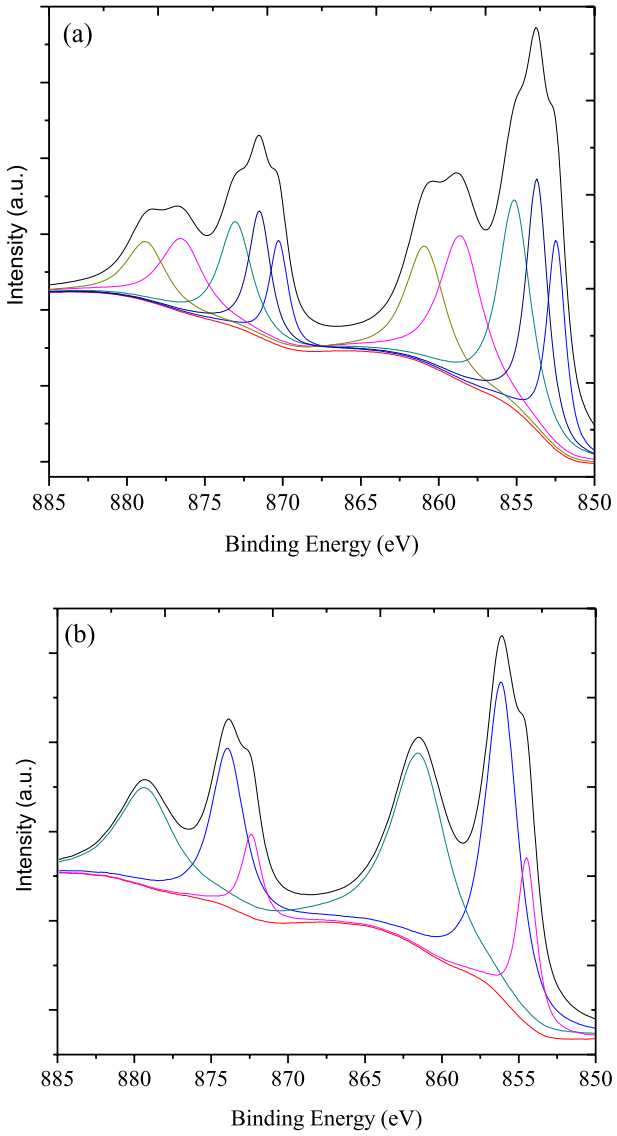

Figure 9. Ni2p core-level spectra: (**a**) Cu catalyst and (**b**) Cu:Ni-2:1 catalyst.

monometallic samples. Experimental results showed that diethyl carbonate reaction rate reached a maximum at 383 K. A rate equation of second order with respect to ethanol and first order to respect carbon dioxide was proposed. This work presents a first kinetic equation to gas phase synthesis to dimethyl carbonate from CO_2 and ethanol and it is expected that this work facilitates a better understanding of the mechanism of the direct synthesis of diethyl carbonate in gas phase, as previous kinetic reports are for the reaction in liquid phase.

Received: 27 December 2023; Accepted: 7 April 2024
Published online: 19 July 2024

References

1. Bashir, M. *et al.* Strontium-based nanomaterials for the removal of organic/inorganic contaminants from water: A review. *Coord. Chem. Rev.* **492**, 215286 (2023).
2. Lee, C. T., Tsai, C. C., Wu, P. J., Yu, B. Y. & Lin, S. T. Screening of CO_2 utilization routes from process simulation: Design, optimization, environmental and techno-economic analysis. *J. CO2 Util.* **53**, 101722 (2021).
3. Han, J. Catalytic syngas production from carbon dioxide of two emission source scenarios: Techno-economic assessment. *J. Ind. Eng. Chem.* **96**, 213–218 (2021).
4. Kim, H., Byun, M., Lee, B. & Lim, H. Carbon-neutral methanol synthesis as carbon dioxide utilization at different scales: Economic and environmental perspectives. *Energy Convers. Manag.* **252**, 115119 (2022).
5. Koohestanian, E., Sadeghi, J., Mohebbi-Kalhori, D., Shahraki, F. & Samimi, A. A novel process for CO_2 capture from the flue gases to produce urea and ammonia. *Energy* **144**, 279–285 (2018).
6. Dai, W.-L., Luo, S.-L., Yin, S.-F. & Au, C.-T. The direct transformation of carbon dioxide to organic carbonates over heterogeneous catalysts. *Appl. Catal. A Gen.* **366**, 2–12 (2009).

7. Putro, W. S. *et al.* Sustainable catalytic synthesis of diethyl carbonate. *ChemSusChem* https://doi.org/10.1002/cssc.202002471 (2020).
8. Jote, B. A. *et al.* Effect of diethyl carbonate solvent with fluorinated solvents as electrolyte system for anode free battery. *J. Power Sources* **461**, 228102 (2020).
9. Li, D., Fang, W., Xing, Y., Guo, Y. & Lin, R. Effects of dimethyl or diethyl carbonate as an additive on volatility and flash point of an aviation fuel. *J. Hazard. Mater.* **161**, 1193–1201 (2009).
10. Schäffner, B., Schäffner, F., Verevkin, S. P. & Börner, A. Organic carbonates as solvents in synthesis and catalysis. *Chem. Rev.* **110**, 4554–4581 (2010).
11. Tan, H. Z. *et al.* Review on the synthesis of dimethyl carbonate. *Catal. Today* **316**, 2–12 (2018).
12. Chen, P., Huang, S., Zhang, J., Wang, S. & Ma, X. Enhanced CuCl dispersion by regulating acidity of MCM-41 for catalytic oxycarbonylation of ethanol to diethyl carbonate. *Front. Chem. Sci. Eng.* **9**, 224–231 (2015).
13. Fan, M., Zhang, P. & Ma, X. Study on Wacker-type catalysts for catalytic synthesis of diethyl carbonate from ethyl nitrite route. *Fuel* **86**, 902–905 (2007).
14. Wang, L. *et al.* Highly efficient synthesis of diethyl carbonate via one-pot reaction from carbon dioxide, epoxides and ethanol over KI-based binary catalyst system. *Appl. Catal. A Gen.* **471**, 19–27 (2014).
15. Décultot, M., Ledoux, A., Fournier-Salaün, M. C. & Estel, L. Kinetic modelling of the synthesis of diethyl carbonate and propylene carbonate from ethanol and 1,2-propanediol associated with CO_2. *Chem. Eng. Res. Des.* **161**, 1–10 (2020).
16. Wang, L. *et al.* The efficient synthesis of diethyl carbonate via coupling reaction from propylene oxide, CO_2 and ethanol over binary PVEImBr/MgO catalyst. *Catal. Today* **281**, 360–370 (2017).
17. Xin, S., Wang, L., Li, H., Huang, K. & Li, F. Synthesis of diethyl carbonate from urea and ethanol over lanthanum oxide as a heterogeneous basic catalyst. *Fuel Process. Technol.* **126**, 453–459 (2014).
18. Dibenedetto, A. *et al.* General synthesis of diethylcarbonate by ethanolysis of urea: A study on the recoverability and recyclability of new Zn-based heterogeneous catalysts. *Appl. Catal. A Gen.* **493**, 1–7 (2015).
19. Shukla, K. & Srivastava, V. C. Diethyl carbonate synthesis by ethanolysis of urea using Ce–Zn oxide catalysts. *Fuel Process. Technol.* **161**, 116–124 (2017).
20. Murugan, C. & Bajaj, H. C. Synthesis of diethyl carbonate from dimethyl carbonate and ethanol using KF/Al_2O_3 as an efficient solid base catalyst. *Fuel Process. Technol.* **92**, 77–82 (2011).
21. Fujita, S., Bhanage, B. M., Arai, M. & Ikushima, Y. Synthesis of dimethyl carbonate from carbon dioxide and methanol in the presence of methyl iodide and base catalysts under mild conditions: Effect of reaction conditions and reaction mechanism. *Green Chem.* **3**, 87–91 (2001).
22. Gasc, F., Thiebaud-Roux, S. & Mouloungui, Z. Methods for synthesizing diethyl carbonate from ethanol and supercritical carbon dioxide by one-pot or two-step reactions in the presence of potassium carbonate. *J. Supercrit. Fluids* **50**, 46–53 (2009).
23. Yoshida, Y., Arai, Y., Kado, S., Kunimori, K. & Tomishige, K. Direct synthesis of organic carbonates from the reaction of CO_2 with methanol and ethanol over CeO_2 catalysts. *Catal. Today* **115**, 95–101 (2006).
24. Prymak, I., Kalevaru, V. N., Wohlrab, S. & Martin, A. Continuous synthesis of diethyl carbonate from ethanol and CO_2 over Ce–Zr–O catalysts. *Catal. Sci. Technol.* **5**, 2322–2331 (2015).
25. Leino, E., Kumar, N., Mäki-arvela, P. & Rautio, A. Synthesis and characterization of ceria-supported catalysts for carbon dioxide transformation to diethyl carbonate. *Catal. Today* **306**, 128–137 (2018).
26. Denardin, F. G. & Valença, G. P. Synthesis of diethyl carbonate from ethanol and CO_2 over ZrO_2 catalysts. *Braz. J. Chem. Eng.* https://doi.org/10.1007/s43153-020-00073-3 (2020).
27. Wang, W., Wang, S., Ma, X. & Gong, J. Crystal structures, acid–base properties, and reactivities of $Ce_xZr_{1-x}O_2$ catalysts. *Catal. Today* **148**, 323–328 (2009).
28. Aouissi, A. & Al-Deyab, S. S. Comparative study between gas phase and liquid phase for the production of DMC from methanol and CO_2. *J. Nat. Gas Chem.* **21**, 189–193 (2012).
29. Arbeláez, O., Orrego, A., Bustamante, F. & Villa, A. L. Direct synthesis of diethyl carbonate from CO_2 and CH_3CH_2OH Over Cu–Ni/AC catalyst. *Top. Catal.* **55**, 668–672 (2012).
30. Bustamante, F. & Arbela, O. Effect of acidity, basicity and ZrO_2 phases of Cu–Ni/ZrO_2 catalysts on the direct synthesis of diethyl carbonate from CO_2 and ethanol. *Catal. Lett.* https://doi.org/10.1007/s10562-016-1699-4 (2016).
31. Arbeláez, O., Hernández, E., González, L. M., Bustamante, F. & Villa, A. L. Enhanced conversion in the direct synthesis of diethyl carbonate from ethanol and CO_2 by process intensification. *Chem. Eng. Technol.* **42**, 1135–1143 (2019).
32. Tayyab, M. *et al.* One-pot in-situ hydrothermal synthesis of ternary $In_2S_3/Nb_2O_5/Nb_2C$ Schottky/S-scheme integrated heterojunction for efficient photocatalytic hydrogen production. *J. Colloid Interface Sci.* **628**, 500–512 (2022).
33. Tayyab, M. *et al.* Simultaneous hydrogen production with the selective oxidation of benzyl alcohols to benzaldehyde by a noble-metal-free photocatalyst VC/CdS nanowires Chinese. *J. Catal.* **43**, 1165–1175 (2022).
34. Bian, J. *et al.* Highly effective synthesis of dimethyl carbonate from methanol and carbon dioxide using a novel copper–nickel/graphite bimetallic nanocomposite catalyst. *Chem. Eng. J.* **147**, 287–296 (2009).
35. Deng, X. *et al.* Surface chemistry of Cu in the presence of CO_2 and H_2O. *Langmuir* **24**, 9474–9478 (2008).
36. Gan, L., Tian, R., Yang, X., Lu, H. & Zhao, Y. Catalytic reactivity of CuNi alloys toward H_2O and CO dissociation for an efficient water à gas shift: A DFT study. *J. Phys. Chem. C* **116**, 745–752 (2012).
37. Orrego-romero, A. F., Arbeláez-pérez, O. F., Bustamante-londoño, F., Luz, A. & Holguín, V. Pelletization of catalysts supported on activated carbon. A case study: Clean synthesis of dimethyl carbonate from methanol and CO_2. *Revista Facultad de Ingeniería Universidad de Antioquia* **66**, 38–47. https://doi.org/10.17533/udea.redin.n78a05 (2016).
38. Chen, H. *et al.* Direct synthesis of dimethyl carbonate from CO_2 and CH_3OH Using 0.4 nm molecular sieve supported Cu–Ni bimetal catalyst. *Chin. J. Chem. Eng.* **20**, 906–913 (2012).
39. Bian, J. *et al.* Direct synthesis of dimethyl carbonate over activated carbon supported Cu-based catalysts. *Chem. Eng. J.* **165**, 686–692 (2010).
40. Bian, J., Xiao, M., Wang, S.-J., Lu, Y.-X. & Meng, Y.-Z. Carbon nanotubes supported Cu–Ni bimetallic catalysts and their properties for the direct synthesis of dimethyl carbonate from methanol and carbon dioxide. *Appl. Surf. Sci.* **255**, 7188–7196 (2009).
41. Leino, E. *et al.* Conventional synthesis methods of short-chain dialkylcarbonates and novel production technology via direct route from alcohol and waste CO_2. *Appl. Catal. A Gen.* **383**, 1–13 (2010).
42. Yu, B., Wu, P., Tsai, C., Lin, S. & Picolinimidate, E. Evaluating the direct CO_2 to diethyl carbonate (DEC) process: Rigorous simulation, techno-economical and environmental evaluation. *J. CO2 Util.* **41**, 101254 (2020).
43. Giram, G. G., Bokade, V. V. & Darbha, S. Direct synthesis of diethyl carbonate from ethanol and carbon dioxide over ceria catalysts. *New J. Chem.* **42**, 17546–17552 (2018).
44. Pérez, O. F. A., Cardozo, S. D., Romero, A. F. O., Holguín, A. L. V. & Bustamante, F. Gas phase synthesis of dimethyl carbonate from CO_2 and CH_3OH over Cu-Ni/AC. A kinetic study. *Rev. Fac. Ing.* https://doi.org/10.17533/udea.redin.20190941 (2020).
45. Khromova, S. A. *et al.* Anisole hydrodeoxygenation over Ni–Cu bimetallic catalysts: The effect of Ni/Cu ratio on selectivity. *Appl. Catal. A Gen.* **470**, 261–270 (2014).
46. Arbeláez, O. *et al.* Mono and bimetallic Cu–Ni structured catalysts for the water gas shift reaction. *Appl. Catal. A Gen.* **497**, 1–9 (2015).

47. Bobadilla, L. F. *et al.* Steam reforming of methanol over supported Ni and Ni–Sn nanoparticles. *Int. J. Hydrog. Energy* **38**, 6646–6656 (2013).
48. Yue, W. *et al.* Schottky junction enhanced H_2 evolution for graphitic carbon nitride–NiS composite photocatalysts. *J. Colloid Interface Sci.* **657**, 133–141 (2024).
49. Liu, Y. *et al.* Single-atom Pt loaded Zinc vacancies ZnO–ZnS induced type-V electron transport for efficiency photocatalytic H_2 evolution. *Solar RRL* **5**, 9–17 (2021).
50. Wei, H. *et al.* In situ growth of Ni_xCu_{1-x} alloy nanocatalysts on redox-reversible rutile $(Nb, Ti)_O4$ towards high-temperature carbon dioxide electrolysis. *Sci. Rep.* **4**, 1–11 (2014).

Acknowledgements

O.A. is thankful to Universidad Cooperativa for Project INV2731. A.L.V. and F.B.L. acknowledge the financial support from Universidad de Antioquia.

Author contributions

The authors contributed in the same way to writing—review & editing the paper.

Competing interests

The authors declare no competing interests.

Additional information

Supplementary Information The online version contains supplementary material available at https://doi.org/10.1038/s41598-024-59070-y.

Correspondence and requests for materials should be addressed to A.N.A.A.

Reprints and permissions information is available at www.nature.com/reprints.

Publisher's note Springer Nature remains neutral with regard to jurisdictional claims in published maps and institutional affiliations.

Open Access This article is licensed under a Creative Commons Attribution 4.0 International License, which permits use, sharing, adaptation, distribution and reproduction in any medium or format, as long as you give appropriate credit to the original author(s) and the source, provide a link to the Creative Commons licence, and indicate if changes were made. The images or other third party material in this article are included in the article's Creative Commons licence, unless indicated otherwise in a credit line to the material. If material is not included in the article's Creative Commons licence and your intended use is not permitted by statutory regulation or exceeds the permitted use, you will need to obtain permission directly from the copyright holder. To view a copy of this licence, visit http://creativecommons.org/licenses/by/4.0/.

© The Author(s) 2024